

Geo-Adaptive Deep Spatio-Temporal predictive modeling for human mobility

Syed Mohammed Arshad Zaidi
University at Buffalo
Buffalo, New York, USA
szaidi2@buffalo.edu

Varun Chandola
University at Buffalo
Buffalo, New York, USA
chandola@buffalo.edu

EunHye Yoo
University at Buffalo
Buffalo, New York, USA
eunhye@buffalo.edu

ABSTRACT

Deep learning approaches for spatio-temporal prediction problems such as crowd-flow prediction assumes data to be of fixed and regular shaped tensor and face challenges of handling irregular, sparse data tensor. This poses limitations in use-case scenarios such as predicting visit counts of individuals' for a given spatial area at a particular temporal resolution using raster/image format representation of the geographical region, since the movement patterns of an individual can be largely restricted and localized to a certain part of the raster. Additionally, current deep-learning approaches for solving such problem doesn't account for the geographical awareness of a region while modelling the spatio-temporal movement patterns of an individual. To address these limitations, there is a need to develop a novel strategy and modeling approach that can handle both sparse, irregular data while incorporating geo-awareness in the model. In this paper, we make use of quadtree as the data structure for representing the image and introduce a novel geo-aware enabled deep learning layer, *GA-ConvLSTM* that performs the convolution operation based on a novel geo-aware module based on quadtree data structure for incorporating spatial dependencies while maintaining the recurrent mechanism for accounting for temporal dependencies. We present this approach in the context of the problem of predicting spatial behaviors of an individual (e.g., frequent visits to specific locations) through deep-learning based predictive model, *GADST-Predict*. Experimental results on two GPS based trace data shows that the proposed method is effective in handling frequency visits over different use-cases with considerable high accuracy.

CCS CONCEPTS

• **Applied Computing** → **Human mobility, Spatio-temporal learning**; • **Computing methodologies** → **Deep Learning, Neural networks**.

KEYWORDS

Human mobility, Deep Learning, Neural Networks, Spatio-temporal Data, Predictive Learning, GPS Data

Permission to make digital or hard copies of all or part of this work for personal or classroom use is granted without fee provided that copies are not made or distributed for profit or commercial advantage and that copies bear this notice and the full citation on the first page. Copyrights for components of this work owned by others than the author(s) must be honored. Abstracting with credit is permitted. To copy otherwise, or republish, to post on servers or to redistribute to lists, requires prior specific permission and/or a fee. Request permissions from permissions@acm.org.
ACMGIS'22, November 2022, Seattle, WA, USA

© 2022 Copyright held by the owner/author(s). Publication rights licensed to ACM.
ACM ISBN 978-1-4503-9999-9/18/06...\$15.00
<https://doi.org/10.1145/1122445.1122456>

ACM Reference Format:

Syed Mohammed Arshad Zaidi, Varun Chandola, and EunHye Yoo. 2022. Geo-Adaptive Deep Spatio-Temporal predictive modeling for human mobility. In *Proceedings of ACM ACM SIGSPATIAL International Conference on Advances in Geographic Information Systems (ACMGIS'22)*. ACM, New York, NY, USA, 11 pages. <https://doi.org/10.1145/1122445.1122456>

1 INTRODUCTION

Mining individuals' mobility patterns is an important research area. Studies related to mining mobility patterns have been useful in diverse applications which includes monitoring public health [2, 6], emergency event detection [15], urban planning [34], and transportation engineering [16]. Literature [28] shows that daily human mobility patterns can be captured as a sequence of locations that individuals visited frequently, as they are the basis of essential travel activities such as going from home to workplace in the morning and coming back to home from work in the evening. Despite differences among individuals, previous studies [5, 10] have shown that large scale human mobility patterns are highly regular and predictable due to circadian patterns and routine daily activities, such as one's journey to work or home. Predicting individuals' future visit counts at different locations can be beneficial to urban planners, policy-makers and other entities such as transportation providers and taxi services.

With the rapid increase in use of mobile phones, internet of things, social media platforms across the world, it is now possible to obtain significantly accurate estimate data involving human movements at several temporal and spatial scales. Mobility data sources such as Global System for Mobiles (GSM) cell-tower, Global Positioning System (GPS) and Wireless (WiFi) network have started to be used more frequently for mining key insights about individuals' mobility patterns. The study [21] provided a brief comparison among data arising from these data sources. GPS based data is of higher resolution as compare to other data type as it provide a more accurate estimate of geographical position of mobile devices.

Spatio-temporal prediction problem has been widely studied as it has wide range of applications such as urban planning, traffic control and public health. Predictive models for human mobility can help us understand the behavior of migration flow between rural and urban areas [24, 26] and the behavioral pattern of movements of individuals' in the presence of natural disasters [14], climate change and conflicts [27]. Predictors developed for this task is responsible not only for capturing both spatial and temporal regularities in human movements, but also capture the irregularities in the routine movements. In addition to this, the impact of auxiliary factors such as weather impact, use of transportation mode, preferential locations etc. on the individual movement patterns can also be captured

by such predictors. Due to high availability of human mobility data with advancements made in the use of deep learning approaches, we have seen unique solutions to predict human movements either at the individual or aggregate level. In this study, we focus on the study of predicting an individual's visit frequency at a finite set of locations using the individual's past mobile phone data. This can be seen to be closest variant of crowd-flow prediction task in crowd traffic forecasting where the task is to predict the inflow (number of people entering a region in a given time) and outflow (number of people leaving a region in a given time) of a region given their past history of flow information.

Some studies [17, 18, 35] have used traditional multiple machine learning techniques to solve this problem in different settings. Deep-learning approaches has been more popularly used modeling approach for tackling this problem over other traditional approaches because it can handle the spatial and temporal dependencies well and can capture the impact of certain external features in increasing the prediction accuracy. Deep learning approaches has been used in tackling this task in reference to different applications. For example, [29] used deep learning in forecasting crime in a fine-grain city partition, while [30] used ST-ResNet [45] to forecast crime distributions over the Los Angeles area. Deep learning approaches have also been used in understanding traffic flow and forecasting traffic accidents. For instance, [43] used ConvLSTM on heterogeneous urban data for forecasting traffic accidents while [22] used ConvLSTM along with Bidirectional LSTM in predicting short-term traffic flow on the urban daily traffic data. Although, these existing approaches have been employed in various ways on the crowd-flow based problems, they still suffer from the following issues:

- (1) **Handling large study area with sparsity** – In general, different studies for crowd-flow based tasks, usually takes the entire area and convert it into raster data format usually into a matrix or tensor. This may not be a problem for a small study area, but when the study area gets large, then the ability to handle such large tensors requires a considerable amount of computational resources. In addition to this, when there may only small target regions that are used by an individual's movement, then we further cause the algorithm to waste its operation on regions that haven't recorded movements. More specifically, we have one individual just having movements recorded near north-east region, while another individual has their movements recorded near south-east. Considering these set of individuals with diverse trajectories, the existing approaches will have to perform extra computations to account for spatial and temporal dependencies.
- (2) **Incorporating geo-awareness while handling irregularity in geographical data** – Another issue is that each tensor, which usually has a frequency of visits attached to each of the cell, doesn't account for any geographical information such as presence of water bodies and other hazards, when making the prediction. To better enhance the prediction of future count visits in important regions, we can enhance the focus on the regions according to the density of visits made by an individual. We make use of varying the coarser and finer resolutions of regions within the geographical area by making use of quad-tree indexing. Specifically,

the regions with more movements would have finer resolution as compare to the regions with fewer movements. This would mean that the specific target regions would end up being irregular gridded which would then pose limitations on the conventional use of the existing deep-learning approaches since most approaches are used to handle fixed and uniform shape of input data.

In summary, handling large study area with sparsity, incorporating geo-awareness while handling irregularity in geographical data and using a more robust evaluation metrics are the issues that require great consideration and requires to be addressed accordingly. In this paper, we have addressed these issues and have made contributions that can be summarized as follows:

- We propose the use of quadtree-based data structure for indexing the regions in a geographical area. This is to handle the different density of visit counts across regions, as some regions will have more density of visit counts as compare to other regions. Here, we also propose the strategy to employ this data structure in a way so that we incorporate the changes in the architectural model.
- We design a novel deep-learning layer called *GA-ConLSTM*, that makes use of geo-awareness module in performing convolutions only in the regions that requires more focus or are more significant in terms of movement patterns of individuals'.

2 BACKGROUND

2.1 Irregular Geographical data

Literature surveys [3, 31] on spatio-temporal data mining provided an overview of taxonomy of different types of data encountered in spatio-temporal problem space. These included *event*, *trajectory*, *point reference* and *raster*. Different types of problems in this space requires us to represent the data differently as inputs to a model. In our work, we are analyzing data in raster or gridded data. Raster data are formed as measurements of a continuous or discrete spatio-temporal field recorded at fixed locations in space and time. To solve problems related to data involving raster format, we can make use of deep learning approaches like convolutional and recurrent neural network to solve the problems. This proved to be beneficial in different applications, however, this has posed certain limitations. For example, there could be use-cases where we encounter the sparse data where only a few regions are activated spatially or temporally. Due to these challenges, it is imperative to find solutions that effectively handles these limitations. In the recent past, many problems have been studied in the context of non-euclidean space that doesn't have restrictions on data to have some form of regular structure. For example, a different type of irregular *gridded* geographic data can be seen in Fig. 1.

Employing use of deep learning approaches such as Convolutional Neural Network (CNN) and Recurrent neural network (RNN) for predicting spatio-temporal prediction problem on irregular geographic gridded data is limited, and it requires certain changes either at the algorithm-level or at data-level. In this work, we address this problem of building spatio-temporal predictor by handling irregular geographic gridded data based on the rectangular polygons obtained from the quad-tree indexing of the target region, such as

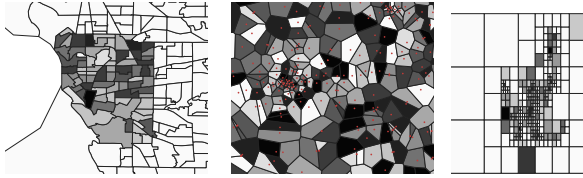


Figure 1: Three typical examples of irregular “gridded” geographic data: a). Each irregular polygon corresponds to an administrative region (census tracts) and the color intensity indicates the number of crime incidents reported within a year, b). Polygons obtained via Voronoi Tessellation from mobile phone tower locations (shown in red); color intensity indicates the daily number of phone calls originating from each tower, and c). Rectangular polygons obtained from quad-tree indexing of the target region; color intensity indicates an individual’s visit frequency (from GPS traces) to each polygon in a given day.

shown in Fig. 1(c). This involves proposing novel strategies both at the data-level and algorithmic-level. We will first present the proposed methods and will then show the of results on GPS-based trace datasets.

2.2 Deep Learning for spatio-temporal prediction

Spatio-temporal data has varying dependencies both at spatial level and temporal level, which poses a considerable limitation to classical data mining methods. Deep learning approaches has been widely used in developing predictive models for human mobility [37, 38, 42, 45]. Predicting future mobility at individual levels is one of the significant problem related to human mobility mining. Major prediction tasks concerned with human mobility can be majorly categorized into either *next-location prediction* or *crowd-flow prediction*. The problem of next location prediction is concerned with predicting the next location to be visited by the user, given their history of past location’s data. This task has been found significant in various applications such as improving travel recommendation [23, 33], geomarketing [9] and link prediction in social networking platforms [46]. Crowd-flow prediction is concerned with predicting the future incoming and outgoing flows of locations in a geographic region, where the region is tessellated into tiles of shapes such as squares, hexagons, etc. This prediction task has significant potential impact for different application use-cases. It can help policymakers, development managers, urban and infrastructure planners in deriving key insights from understanding traffic congestion patterns across time. This can also benefit certain monitoring agencies in preparing and dealing with adverse situations such as crime and accidents in advance. The other benefit can relate to business investment corporations, which can better sense and understand the potential business gains when making investments in a region. Several deep learning based approaches have been widely done in solving this task. Most of the studies employing deep-learning based approaches have achieved considerable success with improvements in prediction accuracy. Approaches such as Convolution neural networks (CNN) and Recurrent neural

networks (RNN) have been used extensively [8, 45] in capturing spatial and temporal movements in crowd-flow prediction task. The study [20] presented the use of both CNN and RNN to capture the spatio-temporal movements. Alternatively, a recent study [36] presented a unique convolution Long-short term network (ConvLSTM) for precipitation nowcasting on radar echo dataset to capture both the spatial and temporal correlation effectively. Specifically, some studies have used multiple machine learning techniques to count prediction problems in different settings, including using deep learning approaches to forecast crime incidents across different spatio-temporal scales. For example, [29] used deep learning in forecasting crime in a fine-grain city partition, while [30] used ST-ResNet [45] to forecast crime distributions over the Los Angeles area.

All of these deep-learning based works haven’t addressed the problem of incorporating geo-awareness and sparsity of visit counts in the study area explicitly. Most of the works have used the study area and converted them into raster format data, which were then fed into the models explicitly. In this paper, we propose the use of quadtree data structure to index regions and created a more focused approach where we will provide a model a way to focus on regions that have been frequently visited as compare to other regions.

3 PROBLEM FORMULATION

For each individual, the raw GPS data is available as a series of chronologically ordered GPS locations (latitude and longitude), denoted as $p_1^{(i)} \rightarrow p_2^{(i)} \rightarrow \dots$, where the index in the superscript, i , denotes the i^{th} individual.

We transform this data into a gridded representation, by first grouping the locations by a individual-specific temporal window, e.g., hourly, daily, weekly, etc. For each window, e.g., a day, we construct a $M \times N$ matrix $X_t^{(i)}$, where M and N are the number of rows and columns, respectively, of a uniform spatial grid of a particular scale, applied on the target spatial area. t denotes the index of the temporal window. Each entry of $X_t^{(i)}$ is equal to the number of times the i^{th} individual’s “visits” the corresponding grid cell, during the t^{th} window. We will refer to the matrix $X_t^{(i)}$ as the *visit count matrix* for the i^{th} individual for the t^{th} time window.

We then transform this data into an irregular gridded representation in the form of quadtrees so that we make use of spatial variability of the distribution of visit counts across different regions. In this paper, we are investigating the visit frequency prediction problem on quadtrees. Here, the visit frequency prediction problem can be defined as follows: *Given the historical visit count quadtrees until time t , denoted as $\{\text{quad}X_j^{(i)}\}_{j=1}^t$, predict the future visit counts quadtrees $\{\text{quad}X_f^{(i)}\}_{f=t+1}^{t+d}$, where $f > t$ and d is the forecasting time steps.*

4 METHODS

In this section, we will first present Quadtrees. Quadtree is a tree-based data structure that can be used to prepare the spatio-temporal raster data. We will then introduce the novel convolution recurrent

layer that makes use of geo-awareness for performing the convolution while maintaining the recurrent mechanism. This ensures that the simultaneous spatial and temporal correlations are considered

4.1 Data Structure

In this work, we first decompose an image with the use of linear quadtree [13]. Quadtrees [12] is a tree data structure where each node has either zero or four children. We represent an image with a quadtree where each of non-zero image pixel regions are divided repeatedly into four quadrants (NW – NorthWest, NE – NorthEast, SW – SouthWest, SE – SouthEast) as shown in Fig. 2

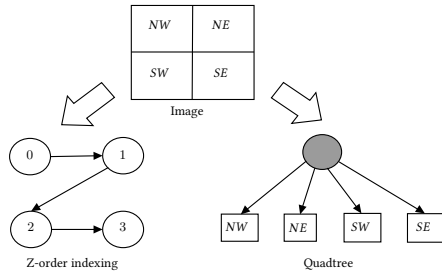


Figure 2: Example of the quadrants of an image in a quadtree

Each of the node in the quadtree is labelled through a *Morton sequencing* [25], a special sequence that is used as an addressing scheme by interleaving binary digits of y and x . The decomposition of an image into quadtree leads to the use of morton sequencing address scheme as shown in Fig. 3. Morton sequencing makes use

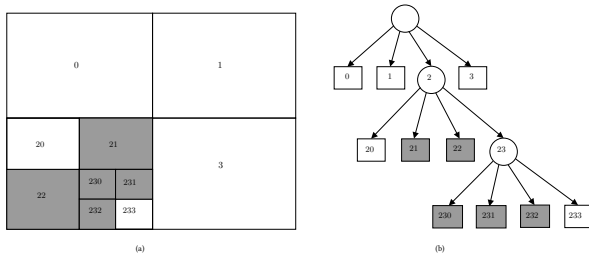


Figure 3: (a) block decomposition (shaded regions contain non-zero pixels while non-shaded regions contain only the zero pixels.) along with corresponding (b) quadtree

of addressing scheme which is equivalent to interleaving of binary representations of x and y coordinates, and we can also obtain its decimal representation. For example, the morton code address of 302 in a quadtree will give the binary representation of row and column coordinates of an image. By interleaving the corresponding binary digits of $y = 101$ and $x = 100$, we get 110010 in binary and 50 in decimal). We choose the morton code address scheme for location indexing while doing the quadtree decomposition of an image.

4.2 Data Preparation

The proposed model consists of first aligning the quadtrees at each level for the raster format data, and then using them as inputs to

the proposed deep learning network architecture. Here, we will first describe the strategy to align the quadtree and then present the data preparation format that we will need to prepare for the training of our deep-learning based model.

4.2.1 Quadtree alignment. The quadtree for each time step or local quadtree would be different, as the visit counts of each user may be different for each day. In order to make use of any deep learning approach for temporal modeling, we need to ensure that we align the quadtrees of each timestep in a way that is effective for the use of any deep learning approach.

In order to address the alignment issue, we first construct a universal quadtree by first aligning all the raster image data available in the training set. We concatenate all the raster image data and form one universal raster image. We then decompose this universal raster image into a universal quadtree. Consequently, we will obtain the quadtree that will have the format as a $\langle key, value \rangle$ where key is the quadnode indexed by morton code and $value$ is shape of the data indexed by the quadnode index, i.e. key . This information will then be used to align the individual quadtrees so that we have uniformity in the number of regions across different quadtrees.

4.2.2 Building relation between quadtree levels. Since the universal quadtree will have nodes at each of the levels, we need to build a relation between nodes at each levels by building a set of nodes we will focus on for preparing the data. For example, if we have universal quadtree that has the following $\{key, value\}$ format which can be equivalently described as

$$\{level : [node\ index\ 1, node\ index\ 2, node\ index\ 3, \dots]\}$$

where $keys$ are the levels, and $values$ are the list of quadnodes at each of those level. Then, we want a list of quadnodes called *universal quadlist*.

This can prove to be useful while preparing the data of each quadtree of a daily raster for each individual in the dataset.

Now, having described the universal quadtrees and universal quadnodes, we can now focus on building the relation between nodes at some current level based on the association between previous and next level. One of the ways is to build a relation between all the levels through some parent-child association strength, or how well-connected a parent node is to their child nodes. This can be understood through the following example – if we have quadnode with morton code of 0 in level 1, then we check if the quad node index starting with 0 at level 2 has 4 children nodes or not. If we have all 4 children nodes at level 2, i.e. 00, 01, 02 and 03, then we include them in the universal quadlist or else we just include the parent node with code 0 at level 1 in the universal quadlist. Similarly, if have morton code of 00 at level 2, then we looked into its children at level 3. If we have all 4 children nodes at level 3, i.e. 000, 001, 002 and 003, then we include them in the universal quadlist or else we stay with the parent node at level 2 and include that in the universal quadlist. This way we build a complete list of nodes at different levels.

4.2.3 Data Transformation. Once we will have these list of nodes from the universal quadtree, we then perform the alignment of (local) quadtree at each timestep with only the list of quadnodes we got from universal quadtree.

We align each of the local quadtrees in terms of quadnode indices for each timestep. While performing the alignment, there will be some issues. These issues can be described as follows:

- If a local quadtree at any given timestep doesn't have a quadnode at a level in comparison to the corresponding quadnode in universal quadtree, then we create the quadnode in the local quadtree by creating a data which will be an array of zeros with data shape retrieved for that quadnode from universal quadtree.
- If a local quadtree at any given timestep does have a quadnode at a level but is not matching in shape with the quadnode corresponding to the universal quadtree, then we pad the data in the quadnode in the local quadtree with zeros to match the shape with quadnode with universal quadtree.

After handling the above issues, we will get an alignment in structure of quadnodes for every local quadtree. Next, we transform the data for quadtrees at every timestep as shown in fig. 4. We arrange the quadnodes in a linear fashion and makes use of $\{key: value\}$ as indicated in fig. 4. We will have a quadnode index (also indicated as qnode_index) as the key and the list of values where values are quadnode data, index_start, index_stop which can be described as below:

- *data_shape*: shape of the data corresponding to quadnode.
- *index_start*: index which indicates the beginning or start position of a given quadnode data array.
- *index_stop*: index which indicates the end or stop position of a given quadnode data array.

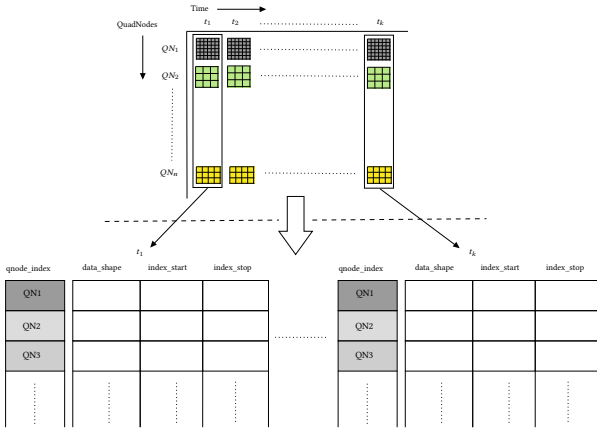


Figure 4: Data preparation format for Training phase

4.3 Model Architecture

Our model comprises the use of a novel geo-aware convolution recurrent layer, called *GA-ConvLSTM* for predicting the future visit frequencies of a user based on its past data. Because the data is prepared according to the quadtree-based data structure, it is required to perform both the input and recurrent convolutions based on the adaptive nature of the geographical area. This will provide us two major advantages – *firstly*, we make use of coupled spatio-temporal dependencies that are adaptive to the geographical area

and *secondly*, the weights are shared as we go along performing the convolution operation on each of the quad nodes.

4.3.1 GA-ConvLSTM. To accommodate both the temporal and spatial dependencies in the data, Shi et al. [36] proposed the Convolutional LSTM (ConvLSTM) that is similar to fully connected LSTM (FC-LSTM) but uses convolution operator in the state-to-state and input-to-state transitions. The usual ConvLSTM equations are described below:

$$\begin{aligned} i_t &= \sigma(W_{xi} * x_t + W_{hi} * h_{t-1} + W_{ci} \circ c_{t-1} + b_i) \\ f_t &= \sigma(W_{xf} * x_t + W_{hf} * h_{t-1} + W_{cf} \circ c_{t-1} + b_f) \\ c_t &= f_t \circ c_{t-1} + i_t \circ \tanh(W_{xc}x_t + W_{hc}h_{t-1} + b_c) \\ o_t &= \sigma(W_{xo} * x_t + W_{ho} * h_{t-1} + W_{co} \circ c_t + b_o) \\ h_t &= o_t \circ \tanh(c_t) \end{aligned}$$

where $*$ denotes the convolution operation and \circ denotes the Hadamard (elementwise) product. Here, i_t, f_t and o_t are the outputs of the input, forget and the output gate respectively. c_t is the cell output at time step, t while h_t is the hidden state of the cell at time step t . σ is the logistic sigmoid function. $W_{xi}, W_{xf}, W_{hi}, W_{hf}, W_{xc}, W_{xo}, W_{ho}, W_{co}$ corresponds to the weight matrices. The usual meaning of each weight parameter matrix is indicative by the subscripts written alongside the symbol (W). For example, W_{hi} is the weight matrix that maps the hidden to input gate. b_i, b_f, b_c, b_o are the bias parameter matrices associated with input gate, forget gate, cell and output gate respectively.

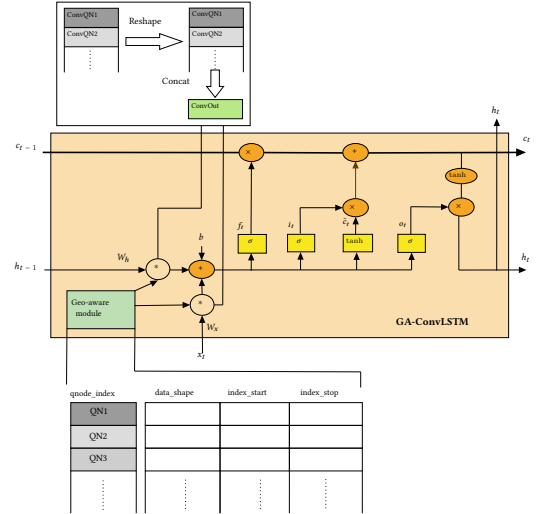


Figure 5: GA-ConvLSTM

The conventional ConvLSTM cell takes the input in a fixed and uniform shape, which has to be consistent throughout each of the input timesteps. This fixed shape prevents us from modelling any inputs that have varying or irregular shapes. In order to accommodate these irregular shapes as inputs, we need to make architectural changes in the convolution operations within the cell. This provided us the motivation for proposing fundamental changes into the structure of a conventional ConvLSTM cell, which can be seen as illustrated in figure 5. We incorporate the use of geo-awareness

that directs the convolution operation based on the geographic region.

4.3.2 Geo-aware module. We construct a novel geo-awareness module that informs the input and recurrent convolution operations based on the geographical area. This awareness module is incorporated through the use of a hash table data structure that has key as quadnode index and value as list which consists of *shape of data within quadnode*, *start_index* and *stop_index*. The indices i.e. *start_index* and *stop_index* are meant to handle the extraction of slices of data. Once a quadnode data slice is extracted, we then reshape it according to the *data_shape* value. After reshaping this, we then perform the input and recurrent convolutions on this data slice. This operation is performed for each of the quadnode data slices. The convolution outputs of these data slices are then aggregated together once the operation is performed in all the slices. Due to the modifications, our expected tensor shapes for long and short-term memory will also have to be modified.

4.3.3 Implementation Details. We first arrange each quadnode and its associated data of a quadtree in a linear sequenced manner. For example, if we have the following quadtree with the following quadnodes and quaddata as shown in figure 6 This way we have a

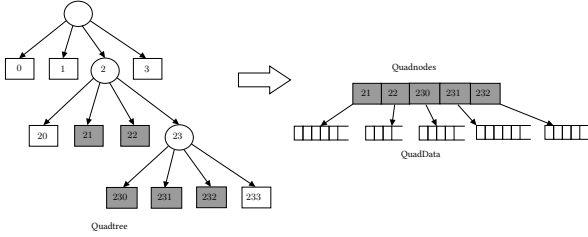


Figure 6: Arranging quadnodes of a local quadtree

large, flattened set of features. The motivation behind building the data like this is to compose the input of shape (*samples*, *timesteps*, *features*). We then passed this input to the GA-ConvLSTM layer.

As the input shape is received, we then make use of geo-awareness module for extracting the data in a sliced manner for each of the region indexed by quadnode index. Each of the sliced data is reshaped into an image format based on the information in *data_shape* provided by the geo-awareness module. Once the data is reshaped, we perform the input and recurrent convolutions on this data slice. The convolution operations is done on different data slice similarly. Once all the quadnode's data have been convolved, we concatenate all the individual convolution outputs or feature maps together as indicated by *ConvOut* in Fig. 5 and pass it to the other gates for further processing. We also change the expected tensor shapes of long-term memory (c_t) and short-term memory (h_t) of the usual cell, as we want to ensure that the recurrent mechanism remains unaffected by the proposed modification.

4.4 Proposed Model

Our proposed model architecture consists of utilizing the novel GA-ConvLSTM layer in predicting future visit counts of individuals, given their past visit counts data. The model architecture can be seen in Fig. 7

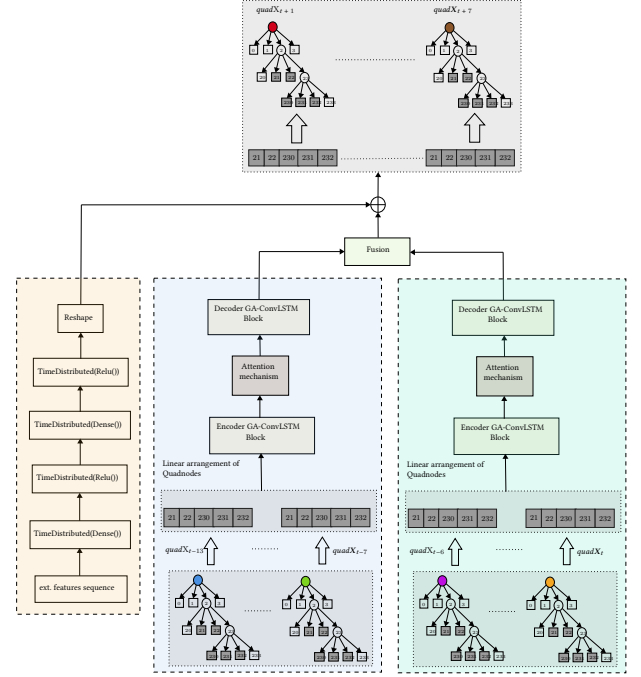


Figure 7: Model Architecture for GADST-Predict

Here, we use the proposed GA-ConvLSTM layer to address incorporate geo-awareness while performing spatial convolution operation on irregular gridded geographical data. In order to effectively capture any complex spatio-temporal patterns within the visit counts of each individual for one week into the future, we use one week history of visit count observations.

User's location visits are affected by external factors such as type of day (Weekday/Weekend), workplace reported (user is working/not working). For example, user's behavior during weekdays will be different from going to some other place during weekends. Similarly, a user's behavior follows some regular pattern going from home to workplace during weekdays while no such regular pattern could be visible during weekends due to irregular spatial and temporal patterns. These metadata features aids the model to learn regular time varying changes in the data. We handle these features through the external component of the model to further enhance the prediction accuracy of visit counts in the future.

4.4.1 GA-ConvLSTM based attention-driven encoder-decoder architecture. The architecture consists of GA-ConvLSTM based attention-driven encoder-decoders that uses past 14 days of historical visit counts data in the quadtree format to forecast the visit counts in the future for 7 days. In order to better forecast the daily visit counts upto 1 week in the future, we use the quadtree data representation of the past two weeks in the following manner:

- Historical data for week before recent past week, i.e.
quadX_{t-13}, quadX_{t-12}, quadX_{t-11}, ..., quadX_{t-7}
- Historical data for recent past week, i.e.
quadX_{t-6}, quadX_{t-5}, quadX_{t-4}, ..., quadX_t

The motivation behind using this is because a simple encoder-decoder scheme may not provide an accurate summary of the past history of observations while we are encoding information as it is restricted to a fixed length of latent vector. By incorporating attention mechanism [4], we account for each of the position of the input sequence while predicting output at each timestep. This makes use of the contribution or influence of each data at each position in correspondence with each output.

The working principle of attention mechanism is following: first, we consider if we have T_x , number of inputs in the sequence; then, the annotations or hidden state outputs are denoted by h_1, h_2, \dots, h_{T_x} . In the simple encoder-decoder model, only the last state (h_{T_x}) of the encoder is used as the context vector and is then passed to the decoder, however, in attention mechanism [4], we compute the context vector c_i for each target output y_i . Each of the context vector c_i is generated using a weighted sum of annotations as:

$$c_i = \sum_{j=1}^{T_x} \alpha_{ij} h_j \quad (1)$$

Here, the weight α_{ij} of each annotation h_j is computed by a softmax function given by the following equation:

$$\alpha_{ij} = \frac{\exp(e_{ij})}{\sum_{k=1}^{T_x} \exp(e_{ik})} \quad (2)$$

where

$$e_{ij} = a(s_{i-1}, h_j) \quad (3)$$

is an alignment model that is responsible for scoring how well the inputs around position j and the output at position i match. It is important to note that the score here depends on the hidden state s_{i-1} , which precedes the output y_i and the j -th annotation h_j of the input sequence.

In terms of architecture in encoder-decoder LSTM block for this component as shown in Fig. 8, the last ConvLSTM layer is followed by a Batch Normalization, Leaky ReLU activation and a dropout layer before feeding to the attention layer. Similarly, on the decoder side, right at the beginning we have a GA-ConvLSTM layer followed by all these layers. A rationale behind using these extra layers is to better capture high-level spatial features temporally, which is best used by the attention layer that improves the representation of the past week's input temporal sequence to generate the relevant output sequence for the following week.

4.4.2 Fusion Layer. We include a final fusion layer that combines the sequence prediction coming from the two components to predict the final output sequence. We compute this output sequence by fusing the sequence outputs of different components of the model with associated learnable component weighted parameters as below:

$$\hat{Y} = W_1 \odot \hat{Y}_1 + W_2 \odot \hat{Y}_2$$

Here, \hat{Y}_1, \hat{Y}_2 are the predicted sequence output coming out of the two components of the model while W_1, W_2 are the trainable weight parameters that indicate the degree of influence that each of the component has on the final sequence prediction.

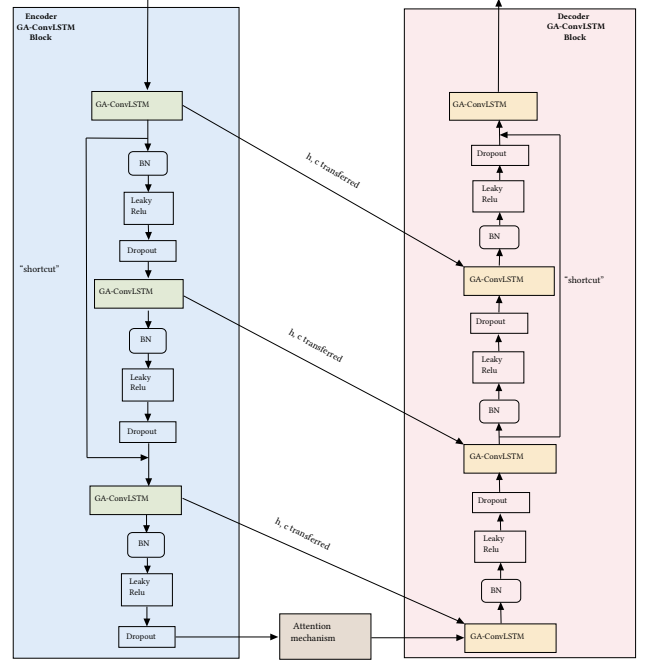


Figure 8: Attention-based encoder decoder

4.4.3 External component. In order to further enhance the performance of the model, we also use external features concerning individuals' within our data. For example, *day of week (week-day/weekend)*, *work reported*, *weather forecast information* etc. We make use of the external data concerning the predicted output sequence from the attention-based encoder-decoder component. To incorporate the external features such as type of day (week-day/weekend) and individuals' demographics such as gender, age etc. as a temporal sequence after the fusion layer, we perform the transformation as shown in Fig. 7. We can represent the external feature sequence as:

$$\text{ext}_{t+1}, \text{ext}_{t+2}, \dots, \text{ext}_{t+7}$$

Here, we used two fully connected (Dense) layers wrapped in a Time Distributed layer. This first fully connected layer ensures that the dense layer is applied to each element of the input sequence. This is followed by a ReLU activation layer, fully connected layer and the subsequent ReLU activation layer. Each of these layers are wrapped within a Time Distributed layer. The first Dense layer acts as an embedding layer on the external features. The second Dense layer is included to map the lower level dimension to the high dimension. We then reshape the output to match with the target output coming from the Fusion layer. Once the reshape is done, we merge the two outputs to get the final prediction sequence as the output.

5 DATASET

The proposed approach is validated through the use of two GPS-based trajectory datasets. The details of the two datasets are described as below:

5.1 Dataset 1

The first data is a private data collected from larger project [11, 39–41]. A total of 1464 participants who were Apple iPhone users were recruited from October 2016 to June 2017. The study area encompasses Buffalo-Niagara region within Erie and Niagara counties of western New York, US. During the study, participants' locations were collected using their own mobile phone and an application developed by our research team. The data has been carefully collected keeping the under the consideration of the privacy of each study participant. Primarily, the data set consists of the following information:

- *Demographics*: It consists of the participants' personal information such as *gender, age group, home and work address, employment status*. In this study, we only use the employment status as an individual-specific feature. In this data set, approximately 17% of the individuals have a non-working status.
- *Global Positioning System (GPS) data*: It consists of the movement locations of participants collected at about 35 minute intervals using the application installed on their mobile phones. The data was collected for a period of 32 weeks in the years of 2016-2017.

5.2 Dataset 2

The data is driven from the GeoLife trajectory dataset [47], a publicly available dataset that was collected in GeoLife project by 182 users in a period of over five years (from April 2007 to August 2012). It contains 17,621 trajectories with a total distance of about 1.2 million kilometers and a total duration of 48,000+ hours. These trajectories were collected using different devices – GPS receivers and GPS-phones, and have a variety of sampling rates. 91 percent of the trajectories are logged in a dense representation, e.g. every 1 ~ 5 seconds or every 5 ~ 10 meters per point. Primarily, the data set consists of the following information:

- *Trajectory data* – Each point in a GeoLife's trajectory contains *latitude, longitude, altitude, and the timestamp*.
- *Other related information* – It also contains the user's transportation mode for most of the trajectories. This recoded a broad range of users' outdoor movements, including not only life routines like go home and go to work but also some entertainments and sports activities, such as shopping, sightseeing, dining, hiking, and cycling.

6 EXPERIMENTAL SET-UP

In the data, there were missing data that needed to be handled before proceeding to the training phase. This included missing data for days in a sequence for a person. We imputed the values of the missing data with the mean value across each corresponding day of the week. The observed visit counts at each location were scaled to the range [0, 1]. While evaluating with the ground truth values, the prediction values are re-scaled back to the normal range. The experiments were conducted on a computing cluster available through Centre for Computational Research (CCR) in University at Buffalo. The nodes equipped with NVIDIA Tesla V100 GPUs with 16GB memory. We used *Keras* library [7] with *Tensorflow* library [1] as the backend.

6.1 Model Training

In Dataset 1, each of 1,464 participants has GPS data records over a maximum period of 221 days (approx. 32 weeks), although some participants had less than 221 days. On average, participants' GPS data were available on 179 days with a minimum of 53 days. Since only 17% of the 1464 participants had non-working status, we selected data for 10 out of 1464 participants across 32 weeks in a way so that the total participants indicated a well-balanced distribution of working and non-working status. We alternatively select participants based on this criteria i.e. out of 485 participants, every alternate participant has a non-working status. We train our model using the 60% of data for each of selected individuals. The model was validated with the remaining 40% data for each selected individuals. The description of the data of users used for experimental evaluation is shown in Table 1. The external features used here is Day of week (Weekday/Weekend) and Work Reported

User	Time period	#days	#Weekdays	#Weekends	#Missing Weekdays	#Missing Weekends
0	2016/10/24 – 2017/06/04	224	160	64	8	4
1	2016/10/25 – 2017/05/21	209	149	60	5	8
2	2016/10/25 – 2017/06/01	220	158	62	16	26
3	2016/10/25 – 2017/06/04	223	159	64	22	7
4	2016/10/25 – 2017/06/04	223	159	64	25	11
5	2016/10/25 – 2017/05/02	190	136	54	18	16
6	2016/10/25 – 2017/06/04	223	159	64	7	3
7	2016/10/26 – 2017/06/04	222	158	64	6	4
8	2016/10/26 – 2017/05/10	197	141	56	5	1
9	2016/10/26 – 2017/06/04	222	158	64	4	1
10	2016/10/26 – 2017/05/22	209	149	60	11	5

Table 1: Information about users in Dataset 1

In Dataset 2, we first selected the participants with data for most consecutive number of days. The objective here was to check whether the model is improving in the absence of any missing data and there is regularity in temporal sequence. After the selection, we selected the users with ID 4, 25, 30, 41 and 68. The description of the data of users used for experimental evaluation is shown in Table 2. We train our model using the 60% of data for each of selected individuals. The model was validated with the remaining 40% data for each selected individuals. The external features used here is Day of week (Weekday/Weekend)

User	Time period	#days	#Weekdays	#Weekends/Holidays
4	2009/04/01 – 2009/07/29	120	84	36
25	2009/03/30 – 2009/06/12	75	53	22
30	2009/04/01 – 2009/07/29	120	84	36
41	2009/04/06 – 2009/07/12	98	68	30
68	2009/05/24 – 2009/08/11	80	56	24

Table 2: Detailed information about users in Dataset 2

6.2 Choosing Hyperparameters

In the attention-based encoder-decoder part, all the ConvLSTM layers has 40 filters on both the encoder and decoder, with the final ConvLSTM layer in the decoder having 1 filter. Each of the filter is of size 3×3 for extracting the relevant spatial features from both the input and output from the previous timesteps. Between each convLSTM layer we have employed a batch normalization layer which is followed by Leaky ReLU and dropout layers. The dropout layer is set with the rate of 0.25. For the external component, we choose 10 as the number of units for the first Dense layer.

6.3 Model Training

We train our model using the training data with batch size of 16 and 300 epochs. We used Adam [19] optimizer with learning rate of 0.001. The optimizer is set with $\beta_1 = 0.9$, $\beta_2 = 0.999$, $\epsilon = 1e - 07$ and clip value = 1.0. We also used model checkpoint that only saves the best weights while training.

6.4 Loss Function

Mean squared error (MSE) is a typical choice for the loss function, in the context of deep learning networks. However, by design, this loss function is biased towards large values, since the square term implies that when there are larger prediction mistakes then the model is punished more than as compare to having smaller prediction mistakes and in order to avoid the prediction being dominated by large values, because of which we also use an additional mean absolute percentage error. Loss function, \mathcal{L} for training the model is composed of Mean Square error (MSE) and square of the Mean Absolute Percentage Error (MAPE).

$$\mathcal{L}(\theta) = \frac{\lambda_1}{N} \sum_{i=1}^N (Y_i - \hat{Y}_i)^2 + \frac{100 * \lambda_2}{N} * \sum_{i=1}^N \left(\frac{Y_i - \hat{Y}_i}{Y_i} \right)^2$$

Here, θ are all the parameters that needs to be learned in the network and λ_1 and λ_2 are the hyperparameters. In all our experiments, we choose $\lambda_1 = 10$ and $\lambda_2 = 100$.

7 RESULTS AND EVALUATION

In this section, we will first discuss results of evaluating the model on the given two datasets. Subsequently, we will discuss the comparison of our proposed model approach with other competitive baseline approach. We use the evaluation metrics, normalized precision (norm_precision) and normalized recall (norm_recall) as proposed in our previous study [44] and described in the appendix section on evaluation measure.

7.1 Results on Dataset 1

The results for Dataset 1 are summarized in Table 3. Overall, the normalized precision is greater than the normalized recall across different prediction horizons. The evaluation measure is consistent as we increase the forecasting horizon from $f = 1$ to $f = 7$.

Type	Metric	f = 1	f = 2	f = 3	f = 4	f = 5	f = 6	f = 7
Overall	norm_Precision	0.44 ± 0.16	0.41 ± 0.17	0.42 ± 0.17	0.43 ± 0.17	0.43 ± 0.18	0.45 ± 0.19	0.47 ± 0.20
	norm_Recall	0.31 ± 0.26	0.32 ± 0.27	0.32 ± 0.27	0.31 ± 0.27	0.30 ± 0.27	0.29 ± 0.28	0.28 ± 0.27
Weekdays	norm_Precision	0.45 ± 0.16	0.43 ± 0.17	0.44 ± 0.17	0.44 ± 0.17	0.45 ± 0.18	0.48 ± 0.19	0.49 ± 0.19
	norm_Recall	0.33 ± 0.26	0.33 ± 0.27	0.34 ± 0.27	0.33 ± 0.27	0.31 ± 0.27	0.31 ± 0.28	0.29 ± 0.27
Weekends	norm_Precision	0.40 ± 0.16	0.39 ± 0.17	0.39 ± 0.17	0.39 ± 0.16	0.38 ± 0.17	0.39 ± 0.18	0.42 ± 0.21
	norm_Recall	0.26 ± 0.26	0.28 ± 0.27	0.28 ± 0.27	0.26 ± 0.27	0.25 ± 0.26	0.24 ± 0.28	0.21 ± 0.25

Table 3: Evaluation of prediction on Dataset 1 for different forecasting horizons (indicated as f). Each value represents the mean ± standard deviation. Overall means including both weekdays and weekends.

7.2 Results on Dataset 2

The results on the given data are summarized in table 4. We observed that the model is able to predict the future visit counts effectively, although, the model is able to perform much better during weekdays as compare to weekends. This can be attributed to

the fact that we have more number of weekdays as compare to weekends.

Type	Metric	f = 1	f = 2	f = 3	f = 4	f = 5	f = 6	f = 7
Overall	norm_Precision	0.48 ± 0.27	0.50 ± 0.24	0.45 ± 0.23	0.47 ± 0.26	0.46 ± 0.27	0.39 ± 0.23	0.31 ± 0.22
	norm_Recall	0.51 ± 0.33	0.49 ± 0.31	0.52 ± 0.32	0.48 ± 0.33	0.49 ± 0.34	0.50 ± 0.34	0.51 ± 0.35
Weekdays	norm_Precision	0.49 ± 0.26	0.51 ± 0.23	0.46 ± 0.23	0.51 ± 0.27	0.48 ± 0.27	0.43 ± 0.25	0.33 ± 0.23
	norm_Recall	0.58 ± 0.36	0.54 ± 0.34	0.59 ± 0.35	0.56 ± 0.36	0.58 ± 0.37	0.57 ± 0.36	0.60 ± 0.37
Weekends	norm_Precision	0.48 ± 0.27	0.49 ± 0.24	0.43 ± 0.24	0.41 ± 0.23	0.44 ± 0.26	0.34 ± 0.20	0.28 ± 0.19
	norm_Recall	0.43 ± 0.26	0.43 ± 0.26	0.42 ± 0.24	0.37 ± 0.23	0.38 ± 0.24	0.39 ± 0.28	0.41 ± 0.28

Table 4: Evaluation of prediction on Dataset 2 for different forecasting horizons (indicated as f). Each value represents the mean ± standard deviation. Overall means including both weekdays and weekends.

7.3 Comparison to baselines

Table 5 presents the performance evaluation of our proposed model with other approaches for spatial resolution of 3×3 at $f = 7$ using Dataset 1. Here, for each user, 60% is used as training data and the remaining 40% is used as validation data. The methods used for comparisons are:

Model	Norm. Precision	Norm. Recall
ARIMA	0.14 ± 0.16	0.06 ± 0.15
STResNet [45]	0.13 ± 0.07	0.17 ± 0.09
Res-ConvLSTM [32]	0.26 ± 0.25	0.16 ± 0.22
GADST-Predict	0.47 ± 0.20	0.28 ± 0.27

Table 5: Performance evaluation of our proposed model (in bold) in comparison with other approaches. Each value represents mean ± stddev. This comparison is done using Dataset 1 at $f = 7$.

- (1) **ARIMA** – Autoregressive integrated moving average (ARIMA), also known as Box-Jenkins model, is a popular model used for time-series forecasting. It uses the historical time series for predicting future values in the series.
- (2) **STResNet** [45] – State-of-the-art approach that makes use of convolutional layers and residual networks for spatio-temporal prediction.
- (3) **Res-ConvLSTM** [32] – STResNet based variant that makes use of ConvLSTM layers for spatio-temporal predictions.

The results clearly indicates that our proposed model outperforms the state-of-the-art and competitive baseline approaches in terms of normalized recall and normalized precision.

8 CONCLUSIONS

In this work, we proposed novel methods to address the problems for sparsity in large study area, incorporating geo-awareness while handling irregularity in the geographical data and evaluating of the model with respect to more robust metrics. We conducted our experiments on a public and private GPS-based trace datasets and validated our models thoroughly.

In the future, we will further enhance our existing deep-learning based approach by incorporating time-aware mechanism that can handle irregular temporal sequence. With this integration, spatio-temporal predictors will be more robust for handling challenges of

missing data, which is more often encounter in real-world use-case scenarios.

REFERENCES

- [1] Martín Abadi, Ashish Agarwal, Paul Barham, Eugene Brevdo, Zhifeng Chen, Craig Citro, Greg S. Corrado, Andy Davis, Jeffrey Dean, Matthieu Devin, Sanjay Ghemawat, Ian Goodfellow, Andrew Harp, Geoffrey Irving, Michael Isard, Yangqing Jia, Rafal Jozefowicz, Lukasz Kaiser, Manjunath Kudlur, Josh Levenberg, Dan Mané, Rajat Monga, Sherry Moore, Derek Murray, Chris Olah, Mike Schuster, Jonathon Shlens, Benoit Steiner, Ilya Sutskever, Kunal Talwar, Paul Tucker, Vincent Vanhoucke, Vijay Vasudevan, Fernanda Viégas, Oriol Vinyals, Pete Warden, Martin Wattenberg, Martin Wicke, Yuan Yu, and Xiaoqiang Zheng. 2015. TensorFlow: Large-Scale Machine Learning on Heterogeneous Systems. <http://tensorflow.org/> Software available from tensorflow.org.
- [2] Ane Alberdi, Alyssa Weakley, Maureen Schmitter-Edgcombe, Diane J Cook, Asier Aztiria, Adrian Basarab, and Maitane Barrenechea. 2018. Smart home-based prediction of multidomain symptoms related to Alzheimer's disease. *IEEE journal of biomedical and health informatics* 22, 6 (2018), 1720–1731.
- [3] Gowtham Atluri, Anuj Karpatne, and Vipin Kumar. 2018. Spatio-temporal data mining: A survey of problems and methods. *ACM Computing Surveys (CSUR)* 51, 4 (2018), 1–41.
- [4] Dzmitry Bahdanau, Kyunghyun Cho, and Yoshua Bengio. 2014. Neural machine translation by jointly learning to align and translate. *arXiv preprint arXiv:1409.0473* (2014).
- [5] Hugo Barbosa, Marc Barthelemy, Gourab Ghoshal, Charlotte R James, Maxime Lenormand, Thomas Louail, Ronaldo Menezes, José J Ramasco, Filippo Simini, and Marcello Tomasini. 2018. Human mobility: Models and applications. *Physics Reports* 734 (2018), 1–74.
- [6] Joana M Barros, Jim Duggan, and Dietrich Reibholz-Schuhmann. 2018. Disease mentions in airport and hospital geolocations expose dominance of news events for disease concerns. *Journal of biomedical semantics* 9, 1 (2018), 18.
- [7] François Chollet et al. 2015. Keras.
- [8] Ronald Clark, Sen Wang, Andrew Markham, Niki Trigoni, and Hongkai Wen. 2017. Vidloc: A deep spatio-temporal model for 6-dof video-clip relocalization. In *Proceedings of the IEEE Conference on Computer Vision and Pattern Recognition*. 6856–6864.
- [9] Gérard Cliquet and Jérôme Baray. 2020. *Location-based Marketing: Geomarketing and Geolocation*. John Wiley & Sons.
- [10] Andrea Cuttone, Sune Lehmann, and Marta C González. 2018. Understanding predictability and exploration in human mobility. *EPJ Data Science* 7, 1 (2018), 2.
- [11] Youngseob Eum and EunHye Yoo. 2021. Using GPS-enabled mobile phones to evaluate the associations between human mobility changes and the onset of influenza illness. *Spatial and Spatio-temporal Epidemiology* (2021), 100458.
- [12] Raphael A. Finkel and Jon Louis Bentley. 1974. Quad trees a data structure for retrieval on composite keys. *Acta informatica* 4, 1 (1974), 1–9.
- [13] Irene Gargantini. 1982. An effective way to represent quadtrees. *Commun. ACM* 25, 12 (1982), 905–910.
- [14] Clark L Gray and Valerie Mueller. 2012. Natural disasters and population mobility in Bangladesh. *Proceedings of the National Academy of Sciences* 109, 16 (2012), 6000–6005.
- [15] Kathryn Gray, Daniel Smolyak, Sarkhan Badirli, and George Mohler. 2018. Coupled IGMM-GANs for deep multimodal anomaly detection in human mobility data. *arXiv preprint arXiv:1809.02728* (2018).
- [16] Zhiren Huang, Ximan Ling, Pu Wang, Fan Zhang, Yingping Mao, Tao Lin, and Fei-Yue Wang. 2018. Modeling real-time human mobility based on mobile phone and transportation data fusion. *Transportation research part C: emerging technologies* 96 (2018), 251–269.
- [17] Yiannis Kamarianakis and Poullicos Prastacos. 2003. Forecasting traffic flow conditions in an urban network: Comparison of multivariate and univariate approaches. *Transportation Research Record* 1857, 1 (2003), 74–84.
- [18] Yiannis Kamarianakis and Poullicos Prastacos. 2005. Space-time modeling of traffic flow. *Computers & Geosciences* 31, 2 (2005), 119–133.
- [19] Diederik P Kingma and Jimmy Ba. 2014. Adam: A method for stochastic optimization. *arXiv preprint arXiv:1412.6980* (2014).
- [20] Chuankun Li, Pichao Wang, Shuang Wang, Yonghong Hou, and Wanqing Li. 2017. Skeleton-based action recognition using LSTM and CNN. In *2017 IEEE International Conference on Multimedia & Expo Workshops (ICMEW)*. IEEE, 585–590.
- [21] Miao Lin and Wen-Jing Hsu. 2014. Mining GPS data for mobility patterns: A survey. *Pervasive and mobile computing* 12 (2014), 1–16.
- [22] Yipeng Liu, Haifeng Zheng, Xinxin Feng, and Zhonghui Chen. 2017. Short-term traffic flow prediction with Conv-LSTM. In *2017 9th International Conference on Wireless Communications and Signal Processing (WCSP)*. IEEE, 1–6.
- [23] R Logesh and V Subramaniaswamy. 2019. Exploring hybrid recommender systems for personalized travel applications. In *Cognitive informatics and soft computing*. Springer, 535–544.
- [24] Massimiliano Luca, Gianni Barlacchi, Nuria Oliver, and Bruno Lepri. 2021. Leveraging Mobile Phone Data for Migration Flows. *arXiv preprint arXiv:2105.14956* (2021).
- [25] Guy M Morton. 1966. A computer oriented geodetic data base and a new technique in file sequencing. (1966).
- [26] Rafael Prieto Curiel, Luca Pappalardo, Lorenzo Gabrielli, and Steven Richard Bishop. 2018. Gravity and scaling laws of city to city migration. *PLoS one* 13, 7 (2018), e0199892.
- [27] Rafael Reuveny. 2007. Climate change-induced migration and violent conflict. *Political geography* 26, 6 (2007), 656–673.
- [28] Chaoming Song, Tal Koren, Pu Wang, and Albert-László Barabási. 2010. Modelling the scaling properties of human mobility. *Nature Physics* 6, 10 (2010), 818.
- [29] Alexander Stec and Diego Klabjan. 2018. Forecasting Crime with Deep Learning. *arXiv preprint arXiv:1806.01486* (2018).
- [30] Bao Wang, Duo Zhang, Duanhao Zhang, P Jeffery Brantingham, and Andrea L Bertozzi. 2017. Deep learning for real time crime forecasting. *arXiv preprint arXiv:1707.03340* (2017).
- [31] Senzhang Wang, Jiannong Cao, and Philip S Yu. 2019. Deep learning for spatio-temporal data mining: A survey. *arXiv preprint arXiv:1906.04928* (2019).
- [32] Hong Wei, Hao Zhou, Jangan Sankaranarayanan, Sudipta Sengupta, and Hanan Samet. 2018. Residual convolutional lstm for tweet count prediction. In *Companion Proceedings of the The Web Conference 2018*. International World Wide Web Conferences Steering Committee, 1309–1316.
- [33] Ruizhi Wu, Guangchun Luo, Qinli Yang, and Junming Shao. 2018. Learning individual moving preference and social interaction for location prediction. *IEEE Access* 6 (2018), 10675–10687.
- [34] Feng Xia, Jinhong Wang, Xiangjie Kong, Zhibo Wang, Jianxin Li, and Chengfei Liu. 2018. Exploring human mobility patterns in urban scenarios: A trajectory data perspective. *IEEE Communications Magazine* 56, 3 (2018), 142–149.
- [35] Peng Xie, Tianrui Li, Jia Liu, Shengdong Du, Xin Yang, and Junbo Zhang. 2020. Urban flow prediction from spatiotemporal data using machine learning: A survey. *Information Fusion* 59 (2020), 1–12.
- [36] SHI Xingjian, Zhouong Chen, Hao Wang, Dit-Yan Yeung, Wai-Kin Wong, and Wang-chun Woo. 2015. Convolutional LSTM network: A machine learning approach for precipitation nowcasting. In *Advances in neural information processing systems*. 802–810.
- [37] Feng Xiong, Xingjian Shi, and Dit-Yan Yeung. 2017. Spatiotemporal modeling for crowd counting in videos. In *Proceedings of the IEEE International Conference on Computer Vision*. 5151–5159.
- [38] Huaxiu Yao, Fei Wu, Jintao Ke, Xianfeng Tang, Yitian Jia, Siyu Lu, Pinghua Gong, Jieping Ye, and Zhenhui Li. 2018. Deep multi-view spatial-temporal network for taxi demand prediction. In *Thirty-Second AAAI Conference on Artificial Intelligence*.
- [39] Eun-hye Yoo. 2019. How short is long enough? Modeling temporal aspects of human mobility behavior using mobile phone data. *Annals of the American Association of Geographers* 109, 5 (2019), 1415–1432.
- [40] Eun-hye Yoo, Qiang Pu, Youngseob Eum, and Xiangyu Jiang. 2021. The Impact of Individual Mobility on Long-Term Exposure to Ambient PM_{2.5}: Assessing Effect Modification by Travel Patterns and Spatial Variability of PM_{2.5}. *International Journal of Environmental Research and Public Health* 18, 4 (2021), 2194.
- [41] Eun-Hye Yoo, John E Roberts, Youngseob Eum, and Youdi Shi. 2020. Quality of hybrid location data drawn from GPS-enabled mobile phones: Does it matter? *Transactions in GIS* 24, 2 (2020), 462–482.
- [42] Quan Yuan, Wei Zhang, Chao Zhang, Xinhe Geng, Gao Cong, and Jiawei Han. 2017. PRED: periodic region detection for mobility modeling of social media users. In *Proceedings of the Tenth ACM International Conference on Web Search and Data Mining*. ACM, 263–272.
- [43] Zhuoning Yuan, Xun Zhou, and Tianbao Yang. 2018. Hetero-convlstm: A deep learning approach to traffic accident prediction on heterogeneous spatio-temporal data. In *Proceedings of the 24th ACM SIGKDD International Conference on Knowledge Discovery & Data Mining*. ACM, 984–992.
- [44] Syed Mohammed Arshad Zaidi, Varun Chandola, and Eun-Hye Yoo. 2021. DST-Predict: Predicting Individual Mobility Patterns From Mobile Phone GPS Data. *IEEE Access* 9 (2021), 167592–167604.
- [45] Junbo Zhang, Yu Zheng, and Dekang Qi. 2017. Deep spatio-temporal residual networks for citywide crowd flows prediction. In *Thirty-First AAAI Conference on Artificial Intelligence*.
- [46] Xin Zheng, Jialong Han, and Aixun Sun. 2018. A survey of location prediction on twitter. *IEEE Transactions on Knowledge and Data Engineering* 30, 9 (2018), 1652–1671.
- [47] Yu Zheng, Xing Xie, Wei-Ying Ma, et al. 2010. Geolife: A collaborative social networking service among user, location and trajectory. *IEEE Data Eng. Bull.* 33, 2 (2010), 32–39.

A EVALUATION MEASURE

To evaluate the predictive power of the proposed model to correctly identify the visit locations for a given individual, we need evaluation metrics that can measure the following two aspects:

- (1) **Recall** - *What fraction of actual visits were correctly predicted by the model?*
- (2) **Precision** - *What fraction of the predicted visits corresponded to the actual visits made by the individual?*

Mathematically, the two quantities can be calculated as follows. Consider a $(M \times N)$ test image matrix, X , at a given spatial scale, and let \widehat{X} be the corresponding prediction matrix, obtained from the model. Note that we have dropped the time subscript, t , for clarity. The recall and precision are defined as:

$$\text{recall} = \frac{\sum_{i,j=1}^{M,N} \min(X_{ij}, \widehat{X}_{ij})}{\sum_{i,j=1}^{M,N} X_{ij}} \quad (1)$$

$$\text{precision} = \frac{\sum_{i,j=1}^{M,N} \min(X_{ij}, \widehat{X}_{ij})}{\sum_{i,j=1}^{M,N} \widehat{X}_{ij}} \quad (2)$$

Note that, for both recall and precision, the numerator is the same and counts the overlap between the true and predicted visit counts for each grid cell. In the paper study, we report the average recall and precision over all daily visit counts matrices in the test data set.

An issue with the recall and precision metrics, as defined in (1) and (2), is that they are dependent on a spatial scale (i.e. resolution) at which the matrices are created. Clearly, the task of predicting visit counts at a coarser resolution is *easier* than predicting visit counts at a finer resolution, and the expected recall and precision values at a coarser resolution are higher than at finer resolution. Consequently, the results obtained at different scales are incomparable. This is a clear shortcoming in the present context, since we are interested in understanding the performance of the proposed model as a function of the spatial scale. To address this issue, we propose scale-invariant versions of the above defined recall and precision metrics.

We first calculate the recall and precision of a naive predictor, which simply distributes the total visits in X uniformly across all the grid cells. The output of the naive predictor, denoted as \widetilde{X} , is calculated as:

$$\widetilde{X}_{ij} = \frac{\sum_{i,j=1}^{M,N} X_{ij}}{M \times N} \quad (3)$$

The base recall and precision for this naive predictor are defined as:

$$\text{base_recall} = \frac{\sum_{i,j=1}^{M,N} \min(X_{ij}, \widetilde{X}_{ij})}{\sum_{i,j=1}^{M,N} X_{ij}} \quad (4)$$

$$\text{base_precision} = \frac{\sum_{i,j=1}^{M,N} \min(X_{ij}, \widetilde{X}_{ij})}{\sum_{i,j=1}^{M,N} \widetilde{X}_{ij}} \quad (5)$$

One can verify that the values for the base_recall and base_precision metrics likely increase as the spatial scale becomes coarser, because the probability of placing a randomly assigned visit to a correct grid cell by the naive predictor is $\frac{1}{M \times N}$, which increases as the scale becomes coarser, i.e., M and N become smaller. We use the

performance of the naive predictor to “normalize” the recall and precision of the proposed model as follows:

$$\text{norm_recall} = \text{recall} - \text{base_recall} \quad (6)$$

$$\text{norm_precision} = \text{precision} - \text{base_precision} \quad (7)$$

Both the normalized recall and precision values are reported when comparing the performance of the proposed model across different scales.